

## RESEARCH ARTICLE

## Substorm evolution of auroral structures

10.1002/2015JA021217

N. Partamies<sup>1,2</sup>, L. Juusola<sup>1</sup>, D. Whiter<sup>1,3</sup>, and K. Kauristie<sup>1</sup>

## Key Points:

- Statistically, 1/3 of all auroral structures are arcs
- Magnetic onset happens prior to morphological changes
- Growth phase starts before optical aurora

## Correspondence to:

N. Partamies,  
noora.partamies@unis.no

## Citation:

Partamies, N., L. Juusola, D. Whiter, and K. Kauristie (2015), Substorm evolution of auroral structures, *J. Geophys. Res. Space Physics*, 120, 5958–5972, doi:10.1002/2015JA021217.

Received 16 MAR 2015

Accepted 19 JUN 2015

Accepted article online 25 JUN 2015

Published online 22 JUL 2015

<sup>1</sup>Arctic Research, Finnish Meteorological Institute, Helsinki, Finland, <sup>2</sup>Department of Geophysics, The University Centre in Svalbard, Longyearbyen, Norway, <sup>3</sup>Department of Physics and Astronomy, University of Southampton, Southampton, UK

**Abstract** Auroral arcs are often associated with magnetically quiet time and substorm growth phases. We have studied the evolution of auroral structures during global and local magnetic activity to investigate the occurrence rate of auroral arcs during different levels of magnetic activity. The ground-magnetic and auroral conditions are described by the magnetometer and auroral camera data from five Magnetometers — Ionospheric radars — All-sky cameras Large Experiment stations in Finnish and Swedish Lapland. We identified substorm growth, expansion, and recovery phases from the local electrojet index (*IL*) in 1996–2007 and analyzed the auroral structures during the different phases. Auroral structures were also analyzed during different global magnetic activity levels, as described by the planetary *Kp* index. The distribution of auroral structures for all substorm phases and *Kp* levels is of similar shape. About one third of all detected structures are auroral arcs. This suggests that auroral arcs occur in all conditions as the main element of the aurora. The most arc-dominated substorm phases occur in the premidnight sector, while the least arc-dominated substorm phases take place in the dawn sector. Arc event lifetimes and expectation times calculated for different substorm phases show that the longest arc-dominated periods are found during growth phases, while the longest arc waiting times occur during expansion phases. Most of the arc events end when arcs evolve to more complex structures. This is true for all substorm phases. Based on the number of images of auroral arcs and the durations of substorm phases, we conclude that a randomly selected auroral arc most likely belongs to a substorm expansion phase. A small time delay, of the order of a minute, is observed between the magnetic signature of the substorm onset (i.e., the beginning of the negative bay) and the auroral breakup (i.e., the growth phase arc changing into a dynamic display). The magnetic onset was observed to precede the structural change in the auroral display. A longer delay of a few minutes was found between the beginning of the growth phase and the first detected auroral structure.

## 1. Introduction

The auroral evolution during substorms was introduced by *Akasofu* [1966] as a local time template for a set of certain recognizable auroral forms. In this template, the evening and premidnight sector is dominated by quiet arcs or substorm growth phase arcs, which were described as east-west elongated stable structures. During a substorm growth phase, equatorward motion of arcs is expected. Substorm onsets and expansions typically take place in the midnight sector. Expansion phase auroral structures were described as bright, dynamic and fast-moving forms. Substorm recovery phase or morning sector aurora was characterized by fading brightness, diffuse, broken, and patchy structures. This visually built remarkable overview was based on ground-based images of auroral activity during ground magnetic disturbances identified as substorms. Thus, this template combines local time, temporal, and geomagnetic activity evolution of the aurora.

As the simplest auroral forms, quiet or stable arcs are well studied [e.g., *Borovsky*, 1993; *Kauristie et al.*, 2001; *Knudsen et al.*, 2001]. They are typically defined as east-west aligned forms extending across the all-sky camera (ASC) field of view, or at least a large part of it, with widths of the order of kilometers to hundreds of kilometers. Arcs are expected to occur in any local time sector throughout the auroral zone latitudes [e.g., *Stringer and Belon*, 1967; *Syrjäsuo and Donovan*, 2004; *Wang et al.*, 2010], but most often they are related to the evening sector or the substorm growth phase [e.g., *Gillies et al.*, 2014]. How the arc occurrence rate changes during substorm evolution, or as a function of increasing magnetic activity in general, is not known.

Apart from auroral arcs, spirals [*Partamies et al.*, 2001], patches, and omega bands [*Syrjäsuo and Donovan*, 2004], mesoscale (scale sizes from about 1 km to about 100 km) auroral forms have been examined in detail in event studies. Their average behavior is extrapolated from the reported individual cases without larger statistical analyses. A recently introduced algorithm for automatic detection of the complexity of the

auroral structures [Partamies *et al.*, 2014] allows large-scale statistical studies of the structural evolution of the aurora in different conditions. By analyzing about 1 million ground-based ASC images captured in Lapland in 1996–2007, our previous study concluded that the behavior of the auroral arciness (i.e., how arc-like the auroral structures appear in images) describes well the diurnal and solar cycle evolution of auroral structures. As a continuous and objective number, the arciness provides thorough information on structural changes beyond the few traditionally used auroral structure classes, such as arcs, patches, and omegas. Only less than 10% of all auroral structures can be classified to generally accepted structure groups [Syrjäsuo and Donovan, 2004]. It was further concluded in our previous study that even though auroral arcs are often related to evening sector aurora, arcs are a common feature in all local time sectors.

In this paper, we examine the distribution of auroral arciness during different levels of magnetic activity to determine how accurate the relationship between auroral arcs and the substorm growth phases and quiet time is, and how the occurrence rate of arcs changes with increasing magnetic activity or during substorm evolution. With this study we aim to characterize the substorm auroral structures and to answer the question of whether an observation of an auroral arc can be used to infer something about the level of magnetospheric activity.

## 2. All-Sky Camera Array

This study uses ground-based auroral camera images from five Lapland camera stations (SOD, MUO, ABK, KIL, and KEV) which are part of the MIRACLE instrument network [Syrjäsuo *et al.*, 1998; Sangalli *et al.*, 2011; Partamies *et al.*, 2007]. The station locations can be seen in the map of Figure 1, and their geographic coordinates are listed in Table 1. The image data were collected during the years 1996–2007 when 3–5 identical cameras were operated simultaneously in a similar imaging mode. The camera setup includes optical filters for the three main auroral emission lines, but in this study we only use the green-filtered data (centered at  $\lambda = 557.7$  nm) captured at 20 s cadence and 1 s exposure time. Several hundreds of thousands of images have been collected per station per imaging season which typically extends from September until April. The pixel resolution of  $512 \times 512$  of a single ASC image gives an average spatial resolution of about 1 km at the auroral height of 110 km.

## 3. Methods for Detecting Substorm Phases and Auroral Arcs

### 3.1. Detection of Substorm Phases

Following the method of Juusola *et al.* [2011], we use the interplanetary magnetic field (IMF) data from the OMNI Web and auroral electrojet index data from the ground magnetometers to identify substorm activity. In their paper, Juusola *et al.* [2011] compared the detected substorm onsets with the ones listed by Frey *et al.* [2004] and concluded that the agreement is good. Instead of the lower envelope curve of the global auroral electrojet index (*AL* index), we here use the lower envelope curve of a local electrojet index calculated from the magnetometer measurements at the five ASC stations in Lapland. A local electrojet index (*IL* index) from the full IMAGE magnetometer network (part of MIRACLE) is often used to capture the magnetic changes in the Fennoscandian and Svalbard sector. *IL* index has been shown to correspond to the global activity (*AL* index) in the midnight sector, at 20–02 UT [Kauristie *et al.*, 1996]. The local index from IMAGE magnetometer chain provides higher spatial resolution and a good meridional coverage in the Fennoscandian sector and thus compares better with the all-sky camera data in the same sector. While the midnight sector covers most of the average imaging hours of the Lapland ASCs, we still want to limit the latitude extent of our index to the camera stations only. The ASC station electrojet index is called  $IL_{ASC}$  in this paper to distinguish from the *IL* index of the full magnetometer network. The  $IL_{ASC}$  index data have been collected during the years 1996–2007. This is the same time period for which the ASC data have been analyzed. Substorm growth, expansion, and recovery phases have been detected in an identical way to the previous *AL* index analysis [Juusola *et al.*, 2011; Partamies *et al.*, 2013]:

1. Growth phase is the period from IMF  $B_z$  southward turn until the substorm onset
2. Substorm onset is an abrupt decrease of  $IL_{ASC}$ . The decrease is required to be steeper than 4 nT/min:
 
$$dIL_{ASC}/dt = (IL_{ASC}(t + 1\text{min}) - IL_{ASC}(t))/\text{min} < -4 \text{ nT/min}$$
3. Expansion phase extends from the substorm onset until the  $IL_{ASC}$  index minimum, which must be less than  $-50$  nT
4. Recovery phase is defined from the  $IL_{ASC}$  index minimum until  $IL_{ASC}$  has recovered to values higher than  $-50$  nT or until a new onset

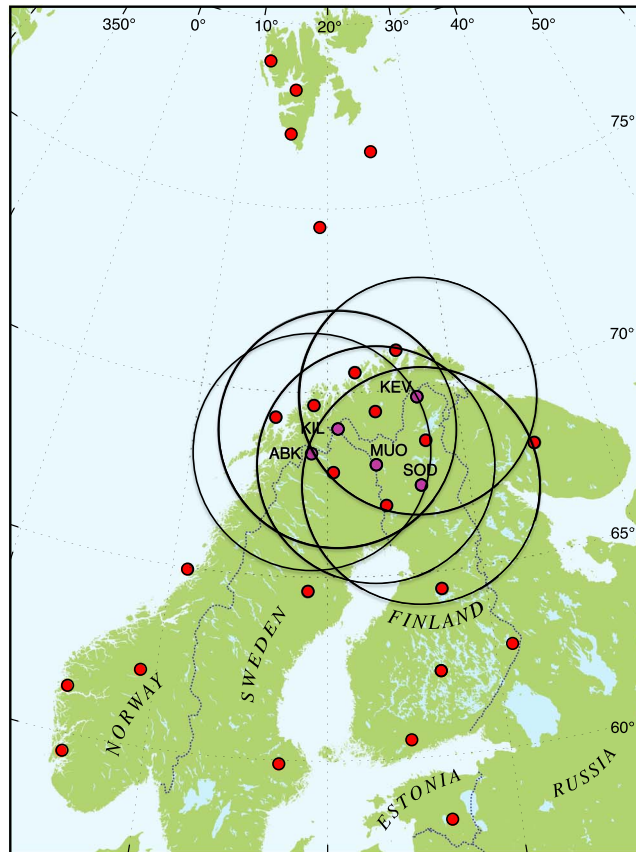


**Figure 1.** Locations of the Magnetometers Ionospheric Radars All-Sky Cameras Large Experiment (MIRACLE) auroral camera stations (named purple spots). Circles around the station locations show the approximate fish-eye field of view; the circle diameter is about 600 km at the altitude of 110 km. The unnamed station locations (red spots) mark the International Monitor for Auroral Geomagnetic Effects (IMAGE) magnetometer stations whose data have been used to calculate the local auroral electrojet index ( $IL$ ).

The minimum  $IL_{ASC}$  value of  $-50$  nT is the median of all negative  $IL_{ASC}$  values over the full  $IL_{ASC}$  data set. Note that the same median value was obtained for the  $AL$  index over the years 1995–2009 [Juusola *et al.*, 2011]. With these criteria, our 12 year period of  $IL_{ASC}$  data included 6518 growth, 16,555 expansion, and 16,067 recovery phases (most substorms consist of multiple expansions and recoveries). This sums up to the total durations of 404 days of growth phase, 254 days of expansion, and 454 days of substorm recovery phase. The median durations of  $IL_{ASC}$  substorm phases were 47 min for growth, 12 min for expansion, and 28 min for the recovery phases, which are—apart from the lengthy growth phases—comparable to the median durations of substorm phases based on  $AL$  index (31, 12, and 31 min for growth, expansion, and recovery Partamies *et al.* [2013]). The median and total durations for all  $IL_{ASC}$  substorm phases in 1996–2007 and the median values for the full IMAGE  $IL/IU$  and  $Dst$  indices during the different phases have been listed in Table 2.

**Table 1.** Names, Geographic Coordinates, and the Years of Operation for the Lapland ASC Stations (From South to North) Used in This Study

Station	Abbreviation	Glat	Glon	Years of operation
Sodankylä	SOD	67.42°	26.39°	2000–2007
Muonio	MUO	68.02°	23.53°	1997–2007
Abisko	ABK	68.36°	18.82°	1997–2002
Kilpisjärvi	KIL	69.02°	20.87°	1997–2007
Kevo	KEV	69.76°	27.01°	1997–2006

**Table 2.** Characteristic Durations and Index Values for all Detected Growth, Expansion, and Recovery Phases<sup>a</sup>

	Growth	Expansion	Recovery
Median duration (min)	47	12	28
Total duration (days)	404	254	454
Median <i>Dst</i> (nT)	−18	−25	−23
Median <i>IL/IU</i> (nT)	−54/44	−165/35	−163/30

<sup>a</sup>These *IL/IU* values are calculated from the full IMAGE magnetometer network.

### 3.2. Auroral Arciness

An arciness value *A* is calculated to estimate the uncertainty in the peak emission height of the aurora by a recently developed method [Whiter *et al.*, 2013]. The arciness is an empirically determined but automatically calculated index *A* which describes how arc-like the dominant structure in an image is. This is done by clustering the brightest pixels and fitting polynomials to the bright pixel regions [Partamies *et al.*, 2014]. The method is insensitive for absolute brightness but requires at least one bright pixel region being detected well above the background. The arciness is a continuous index scaled to range from 0 to 1, so that its maximum value corresponds to an auroral arc or a multiple arc. The lower the *A* value, the more complex the auroral display is. This is due to more bright pixels being scattered to a larger area and located further away from the polynomial fit of the bright pixel region. The calculation of arciness is performed for pruned and paired data which only include images containing aurora and exclude data contaminated by other light sources, such as clouds and twilight. By paired data we mean simultaneous images from two neighboring stations with overlapping fields of view giving a good correlation (Pearson correlation coefficient larger than 0.7 [Whiter *et al.*, 2013]). The required correlation guarantees that the same auroral structure is seen from two stations. This reduces the amount of image data but results in a high-quality data set. The presence of the Moon in images with obvious aurora does not affect arciness because the Moon is such a small object in an all-sky image.

The numbers of images which contain aurora and have been successfully analyzed for arciness in 1996–2007 are 220,420 from SOD, 204,629 from MUO, 103,184 from ABK, 321,804 from KIL, and 242,684 from KEV camera, in total about  $10^6$  images. These are all green line images ( $\lambda = 557.7$  nm) taken at 20 s cadence. The images which contain aurora but have not been included in the analysis are typically very dim, lacking a good contrast for identifying aurora. Thus, some of the excluded images would contribute to the low value end of the *A* distribution.

As concluded by Partamies *et al.* [2014], for clear auroral arc structures arciness equals one. For lower arciness values it is not clear how the structures are organized but they include diffuse aurora, broken and complex structures of active aurora. Thus, our analysis concentrates on the occurrence of arcs ( $A = 1$ ) which is compared to the occurrence of other more complex structures ( $A < 0.9$ ). A set of sample all-sky images with different arciness values is displayed in Figure 2. More example images of different arciness, different bright pixel distributions, and different fitting parameters are presented in our previous paper [Partamies *et al.*, 2014]. In the previous study, the hourly median arciness was observed to decrease steadily from the early evening hours to the late morning hours in a good agreement with earlier studies of auroral local time evolution [e.g., Syrjäsuo and Donovan, 2004]. The years around the solar minimum were reported to be more arc dominated than other years during the solar cycle number 23 [Partamies *et al.*, 2014].

## 4. Results: Arciness at Different Magnetic Activity Levels

### 4.1. Global Activity Described by *Kp* Index

We searched for a planetary *Kp* index value for each auroral image with a successfully calculated arciness. The *Kp* index ranges from 0 to 9 with a 3 hour resolution. The *Kp* value attached to each auroral image is the temporally closest index value, except that during the last 3 hours of the day *Kp* is the last *Kp* of the day (at 21 UT). We further exclude the plus and minus signs of *Kp* but rather only consider the integer value assigned for each 3 hour time slot.

Figure 3 shows the arciness distributions for different *Kp* values from 0 to 9. The shape of the distributions is similar for all levels of global activity. The two maxima are located at arciness values 1 and 0.7;  $A = 1$  corresponds to arcs, and  $A = 0.7$  seems to be a typical value for images where some more broken auroral structures

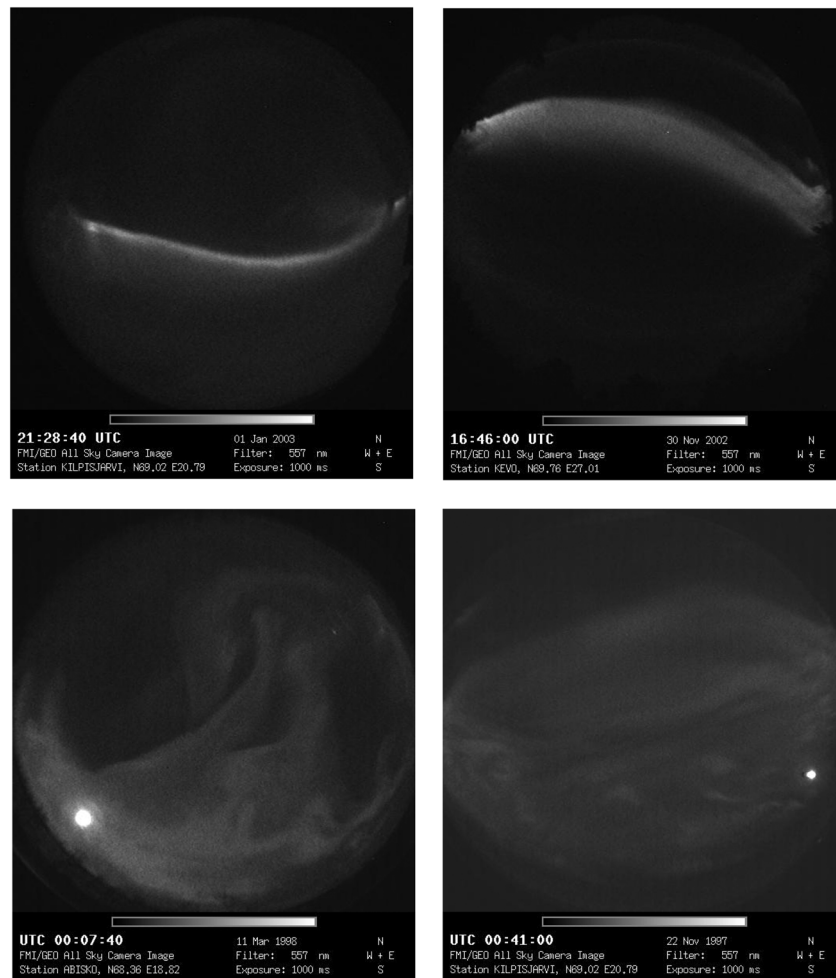


**Figure 2.** Sample ASC images with arciness values of 1.0 and 1.0 in the top panels, 0.8 and 0.6 in the bottom panels.

are seen together with an arc-like structure—a combination which is very common for an all-sky view (see sample images of  $A = 0.7$  in Figure 9).

The median arciness (solid red line on each distribution) varies from 0.76 for  $Kp = 9$  to 0.91 for  $Kp = 2$ .  $Kp$  levels 1 and 2 are related to most arc-dominated aurora, and for higher  $Kp$  the average arciness steadily decreases with increasing  $Kp$ . The lowest  $Kp = 0$  level shows a surprisingly low median arciness, and a maximum at  $A \sim 0.7$  instead of  $A = 1$ . Auroral events during  $Kp = 0$  are mainly from local magnetic midnight hours (19.5–22.5 UT). At  $Kp = 0$ , the auroral oval is located north of Lapland unless there is a substorm taking place [Juusola *et al.*, 2009]. Consequently, more broken structures have been observed in Finland during the lowest activity level. No monthly bias was observed in the  $Kp = 0$  aurora (distributions not shown).

Most auroral observations have been captured during  $Kp = 3$ , which is active enough to bring the nightside auroral oval well above the Lapland stations. The portion of arcs ( $A = 1$ ) for different  $Kp$  levels varies from 20 to 40%. As an exception the fraction of arcs is less than 20% for  $Kp$  values 8 and 9. The same two classes of highest  $Kp$  values ( $Kp = [8, 9]$ ) are the only two magnetic activity levels where the number of analyzed auroral images is less than 10,000. The high number of complex structures during extreme conditions would not be surprising, but the rarity of the high global activity level may skew the arciness distribution somewhat. The fact that on average one third of auroral structures are arcs ( $A = 1$ ) supports the idea that arcs form the main structure element in the aurora and their occurrence are only slightly dependent on the level of global magnetic activity, as suggested by Partamies *et al.* [2014].

The  $Kp$  index distribution for all auroral arcs ( $A = 1$ ) in Figure 4 shows that the moderate activity of  $Kp = 3$  describes the typical conditions for arc observations in the Fennoscandian region. The distribution in the lower

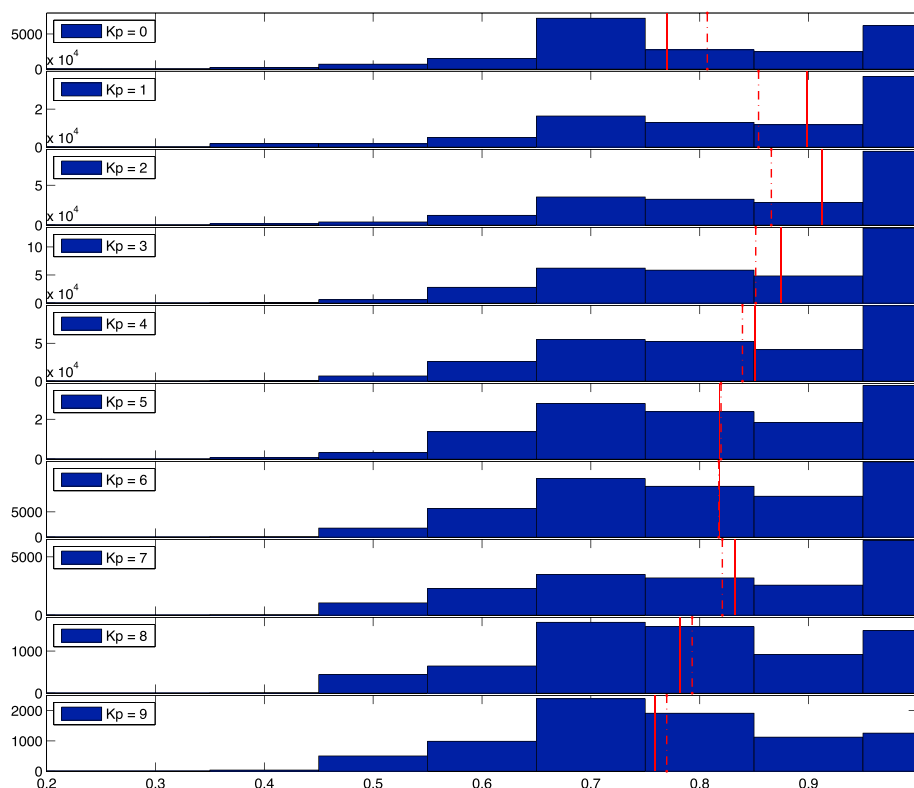


**Figure 3.** (top to bottom) Distributions of arciness for each  $K_p$  index value from 0 to 9. Median  $A$  values are marked by solid vertical lines and mean values by dash-dot lines.

panel is slightly shifted toward higher  $K_p$  level for the more complex auroral structures ( $A < 0.9$ ), but the difference is not large.

#### 4.2. Local Substorm Phases

For each automatically identified local substorm phase we searched for all available  $A$  values. During growth phases 157,098 arciness values were detected, and during expansion and recovery phases we collected 361,122 and 389,604 arciness values, respectively. Many of the identified substorms took place during the summer months or daytime when no auroral image data were available. Our  $A$  values were captured during 2650 growth phases, 7188 expansion phases, and 6635 recovery phases. The total and median duration of these phases and a set of parameters characterizing the aurora during them have been listed in Table 3. It includes the median and total duration of each phase, as well as median  $Dst$  and  $IL/IU$  index values for all detected phases. These numbers are comparable to the median values of magnetic indices and durations reported by *Partamies et al.* [2013] in a statistical substorm study where the global electrojet index ( $AL$ ) was used instead of the local one ( $IL$ ). The growth phases are the longest phases, on average, but there are fewer of them than expansion and recovery phases. The total duration of recovery phases is about twice as long as that of the growth phases.

An example of the temporal evolution of auroral arciness during a sequence of substorms is plotted in Figure 5. These events took place on 24 March in 1998 at 18–24 UT. The top panel arciness (blue asterisks) is from the camera station at Kevo, and the bottom panel arciness (blue) is from the camera station at Abisko. The absolute value of  $IL$  index has been used as a magnetic activity indicator (green curve), which abruptly increases at substorm onsets. For this sample day the substorm onsets (beginnings of expansion phases) have been identified at 20:00, 20:55, and 22:39 UT (vertical dashed lines in the figure). At the onsets the ABK arciness rapidly decreases, although the change at the second onset is much smaller than at the other two. The arciness changes over onsets at KEV are less systematic; at the first onset  $A$  increases, at the second one it decreases a little, and the third onset is associated with a decrease in  $A$  just prior to the onset. Apart from the substorm onsets there are also other fast changes in the arciness values, which makes it hard to visually determine a typical arciness behavior.

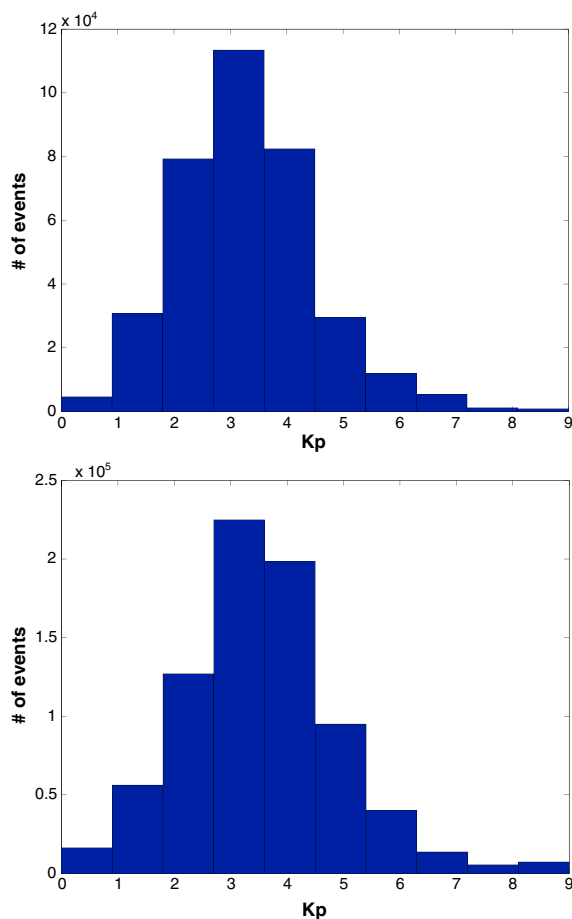


**Figure 4.** Distributions of  $Kp$  index values for (top) auroral arcs ( $A = 1$ ) and (bottom) more complex structures ( $A < 0.9$ ).

growth, 26% during the expansion, and 24% during the recovery phase, which further emphasizes the arc-dominated nature of growth phases but also demonstrates that there is a significant auroral arc population occurring during the expansion and recovery phases as well. In addition to the arciness during the substorms, there were about 200,000 successfully analyzed images which were captured during the quiet time (not shown). This data set behaved similarly to the growth phase arciness in terms of median and mean  $A$  values (0.931 and 0.860, respectively), shape of the distribution, and the number of arcs with respect to other forms (41%). The fact that the quiet time is slightly less arc dominated than the growth phases suggests that the magnetospheric growth phase favors arc formation more than the quiet time does. The growth phase organizes the auroral evolution into a more coherent display prior to a dynamic state of the expansion phase aurora.

By taking one auroral image to represent the auroral structures during 20 s, which is the nominal cadence of the auroral image data, we can estimate the total arc time during each substorm phase. Normalizing the total arc time by the total duration of each substorm phase, during which auroral structures have been observed, results in 8.7% of all growth phase time, 13.2% of all expansion phase time, and 9.2% of all recovery phase time being characterized by auroral arcs ( $A = 1$ ). The numbers are very low because they do not take into account the cloudiness and the fact that aurora is not continuously visible at any given station even during dark, clear skies and substorm activity. However, these percentages give a relative occurrence time of arcs during substorm phases, suggesting that a random image of an auroral arc would most likely be related to a substorm expansion phase.

Figure 7 shows arciness distributions for growth, expansion, and recovery phases in different magnetic local time (MLT) sectors. We have divided the average imaging time into dusk ( $16 < \text{MLT} < 21$ ), midnight ( $21 \leq \text{MLT} \leq 0.5$ ), and dawn ( $0.5 < \text{MLT} < 10$ ), so that the midnight sector corresponds to the local magnetic

We then examine the statistical arciness behavior during substorm phases and with respect to the substorm onsets. The arciness distributions for growth, expansion, and recovery phases of  $IL_{ASC}$  substorms (top to bottom) are plotted in Figure 6. The shape of the distributions is similar in all three phases and resembles the arciness distributions for  $Kp$  from 1 to 7. The highest maximum is seen at  $A = 1$  and a secondary maximum at  $A = 0.7$ . The median arciness for growth, expansion, and recovery phases is 0.979, 0.838, and 0.820, respectively (Table 3). As expected, the growth phase is the most arc dominated of all substorm phases, but the average arciness is rather high during the two latter phases of the substorms as well. The number of expansion and recovery phases are much higher than the number of growth phases. Also, the number of detected auroral structures (successful calculations of  $A$ ) is much higher during expansion and recovery phases as compared to the amount of detected growth phase structures. This is due to the higher occurrence rate of bright aurora during the substorm expansion and recovery phases and larger spatial extent of active auroral display as compared to simple structures but does not explain the excess of arcs ( $A = 1$ ) in the middle of strong or moderate magnetic activity. The percentage of arcs out of all analyzed images is 47% during the

**Table 3.** Arciness Values and Numbers of Successfully Analyzed Auroral Images for All Detected Growth, Expansion, and Recovery Phases<sup>a</sup>

	Growth	Expansion	Recovery
Median <i>A</i>	0.979	0.838	0.820
Number of images	157,098	361,122	389,604
Number of arcs	74,147	95,027	93,323
% of arcs/images	47%	26%	24%
% of arcs/phase duration	8.7%	13.2%	9.2%
Median arc duration (min)	2	1.3	1.3
Median expectation time (min)	5.3	8.3	7.3
Median phase duration (min)	47	23	36
Total phase duration (days)	196	167	236
Median <i>Dst</i> (nT)	-20	-30	-30
Median <i>IL</i> / <i>IU</i> (nT)	-52/49	-204/36	-198/28

<sup>a</sup>The median arc duration and expectation times have been calculated from 3-point median filtered arciness data with maximum of 1 min missing image data. The ratio of the total arc occurrence to the total duration of each phase (%) assumes that each arc image (*A* = 1) represents the arciness for the time period of 20 s, which is the image cadence.

midnight in Fennoscandia and covers the time of typical substorm onset occurrence (90% of the substorms as observed by *Frey et al.* [2004]). Consequently, there are relatively few substorm recoveries in the dusk sector and correspondingly few growth phases in the dawn sector. In general, the recovery phases are the least arc-dominated phases, no matter in which local time sector they occur. The dawn sector is the least arc-dominated sector, no matter which substorm phase we examine. The arciness distribution of dawn sector substorms is also least dependent of the phase in question but shows only little variation between median

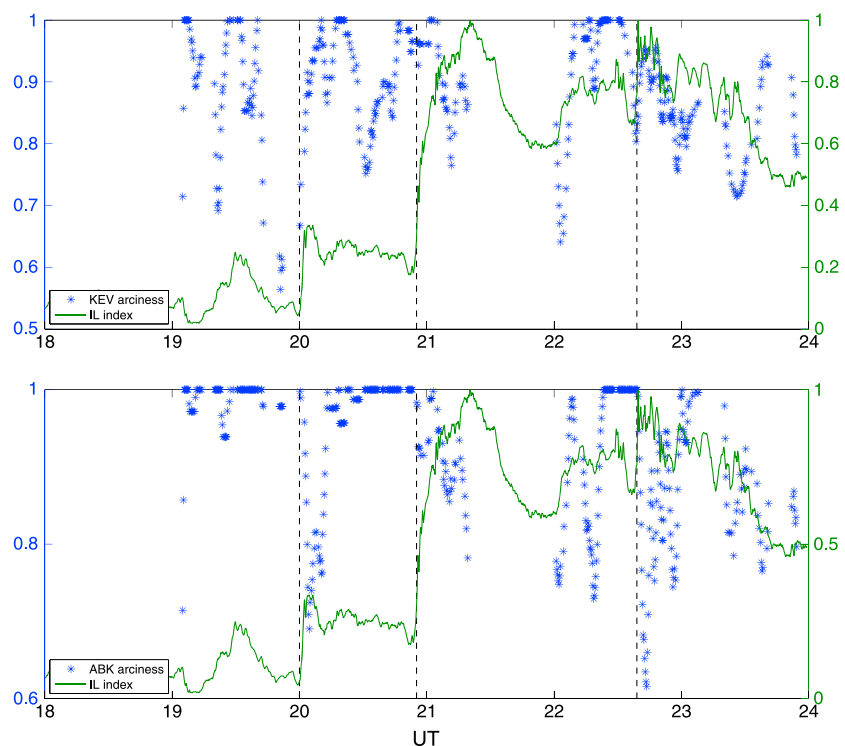


**Figure 5.** An example of the time evolution of *IL* index (green) and auroral arciness (blue) at the stations of (top) KEV and (bottom) ABK on 24 March 1998 at 18–24 UT. An absolute value of *IL* index has been normalized to the range 0–1. Local substorm onsets taking place at about 20:00, 20:55, and 22:39 UT can be seen as abrupt increases in the absolute *IL* index values (vertical dashed lines).

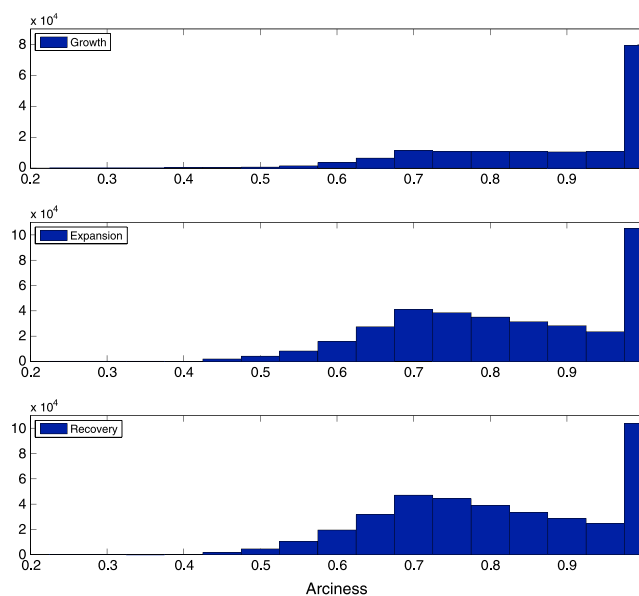


**Figure 6.** Distributions of all arciness values gathered during (top) substorm growth, (middle) expansion, and (bottom) recovery phases.

and mean arciness values (solid and dashed vertical red lines on the histograms) for growth, expansion, and recovery.

#### 4.3. Arc Lifetimes and Onset Evolution

We further examined the lifetime of arcs by identifying sequences of arc events ( $A = 1$ ). This does not provide a mechanism to track single arc structures in the images but just describes how long the all-sky view is dominated by arcs. The image data has a time resolution of 20 s. We smoothed the time series with a three-point median filter to allow single values to be less than 1 and still be included in the same arc event. We further allowed two consecutive missing data points within an arc event. This means that the maximum time separation between two arciness data points within one arc event is 1 min. The procedure resulted in median lifetimes of arcs of 2 min during the growth, 1.3 min during the expansion, and 1.7 min during the recovery phases. The range of the arcs' lifetime extends from 20 s to tens of minutes in each of the different phases. The variability in arc event lifetimes is large, but for 90% of the arc events the lifetime is less than 10 min in growth, less than 7 min in expansion, and less than 9 min in recovery phases. A five-point median filter with the maximum of 2 min of missing data was also calculated, and it resulted in slightly longer arc lifetimes, but the lifetime ratio between the different phases remained the same. The longest-lasting arc events are observed during the growth phases, while the shortest lifetimes of arc events were observed during the expansion phases.

The arc waiting time was defined as the time separation between the end of an arc event and the beginning of the next one. The median values (also given in the Table 3) are 5.3, 8.3, and 7.3 min for growth, expansion, and recovery phases, respectively. This suggests that the arc events during the expansion and recovery phases are both shorter lived and less frequent as compared to the arc events observed during growth phases. There are two ways for an arc event to end: (1) Lack of arciness data, which means a decay of the auroral intensity or the observed arc drifting out of the camera field of view or (2) a deformation of arcs to more complex structures. The decay end (option 1) was found to follow 27% of the arc events during growth phases and 15% of the arc events during the expansion and recovery phases. So even during an arc-dominated growth phase, it is much more common that an already observed auroral arc turns into a more complex structure than that it dies out.

The time evolution of arciness for  $\pm 10$  min from the substorm onsets is plotted in Figure 8. We divided the data set into Arcs ( $A = 1$ , dotted lines) and Others ( $A < 0.9$ , asterisks). The data are displayed with 1 min time resolution. Each 1 min value has been normalized to the full number of images which were successfully analyzed for arciness. The green markers show the occurrence rate of Arcs and Others as calculated from the end of growth phases. Here each time step consists of arciness values from about 1500–4000 individual images. The blue markers describe the occurrence rate for Arcs and Others as determined from the beginning of expansion phases. These data points include about 4000–9000 individual arciness values. Every growth

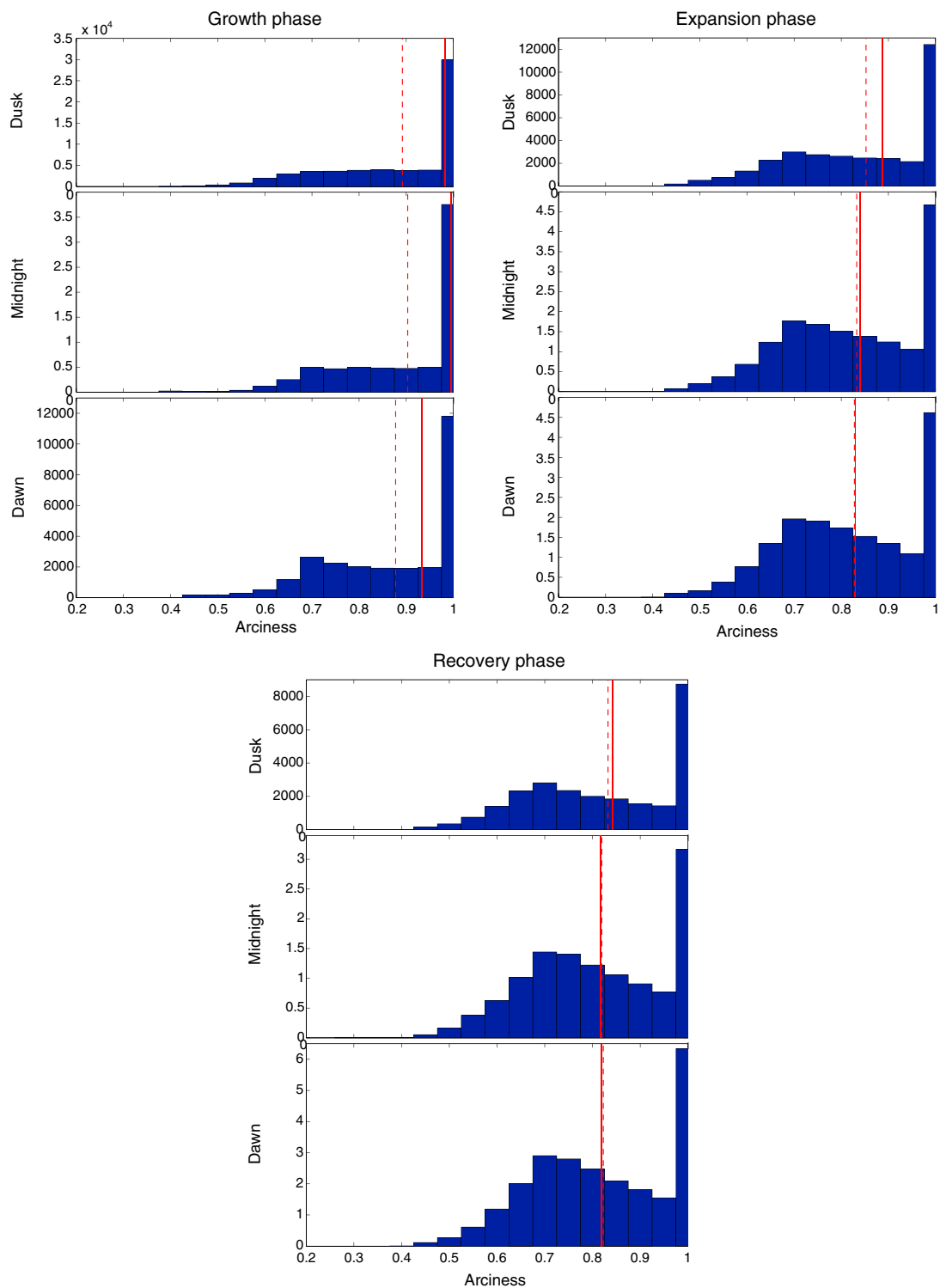


**Figure 7.** Distributions of arciness values gathered during substorm phases in the (top) dusk, (middle) midnight, and (bottom) morning MLT sectors separately. Growth phase arciness (top left), expansion phase arciness (top right) and recovery phase arciness (bottom).

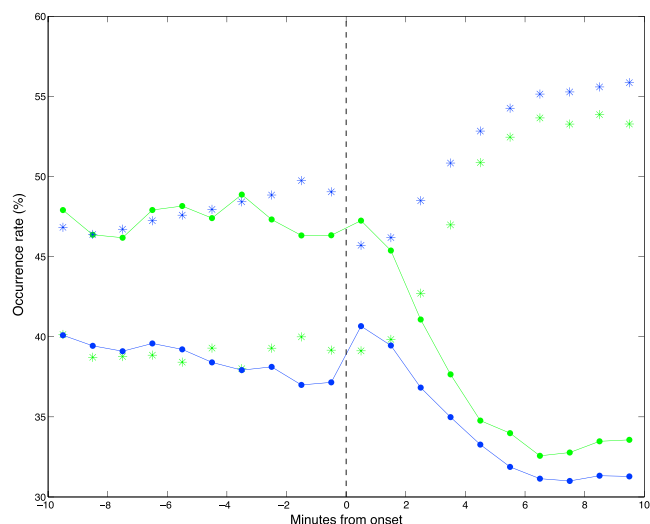


**Figure 8.** The evolution of the occurrence rate of Arcs ( $A = 1$ , dotted curves) and Others ( $A < 0.9$ , asterisks) for an epoch of  $\pm 10$  min from the expansion phase onset (vertical dashed line). The blue (green) markers show the relative occurrence rate (%) of Arcs and Others from the beginnings (ends) of the all expansion (growth) phases. Each 1 min data point has been normalized to the full number of successfully analyzed arciness values. Each minute consists of about 4000–9000 images for the points where the expansion onset is used as the zero epoch time (blue markers). The green markers use the ends of growth phases as the zero epoch time and include about 1500–4000 images.

phase is followed by an expansion phase, but expansion phases can be preceded by recovery phases in addition to growth phases. Thus, the green epochs represent a subset of the blue ones with somewhat higher arc occurrence rate. The temporal variation before the onset is rather steady for both data sets. The strongest arciness gradients are seen 1–6 min after the onset, which is a signature of arc-dominated aurora (majority of the observed structures being arcs) changing to more broken and dynamic structures (majority of observed aurora being more complex structures than arcs). The gentle decrease in arciness within 2 min prior to the onset can be interpreted as the fading of the aurora before the breakup brightening [Kauristie *et al.*, 1995]. Decaying emission brightness would eventually cause loss of detected structures. Consequently, the brightening of the onset arc may contribute to the small increase of arciness right after the onset by making the previously faded arcs visible again. The more complex breakup structures start appearing about 1 min after the brightening when the arciness starts decreasing.

## 5. Discussion

We have examined auroral arciness  $A$  for about 1 million auroral images from five camera stations in Lapland in 1996–2007. The shape of the arciness distributions for all levels of global magnetic activity ( $K_p$ ) and for all substorm phases is similar: about one third of auroral structures are arcs ( $A = 1$ ). In addition, a low, widespread part of the distribution has a secondary maximum at about  $A = 0.7$ . Our analysis consists of the nightside green line aurora, but similar results on arc occurrence rate have been reported by Wang *et al.* [2010] for late morning and early afternoon sectors of the dayside aurora. Obviously, an imager with a smaller field of view (FOV) would see less homogeneous arc-like structures, so the arciness results are only directly comparable with other all-sky observations.

Visual inspection of auroral images with  $A = 0.7$  suggest that this value is related to cases where there is a more complex structure in an image in addition to an arc-like one, or an auroral arc and some partly transparent clouds. These are very common cases in an all-sky field of view. A set of sample images with  $A = 0.7 - 0.8$  are given in Figure 9. Further studies are required to characterize the effect of the camera FOV in this secondary maximum of arciness.

The statistical delay of about 1 min between the magnetic ( $IL_{ASC}$ ) onset and the optical auroral onset may be due to the different fields of view of the cameras and magnetometers. This may be an upper limit of the average time delay limited by the temporal resolution of the MIRACLE ASC data (20 s cadence). As demonstrated by our sample substorm event, arciness varies fast and may behave very differently from one event to another.

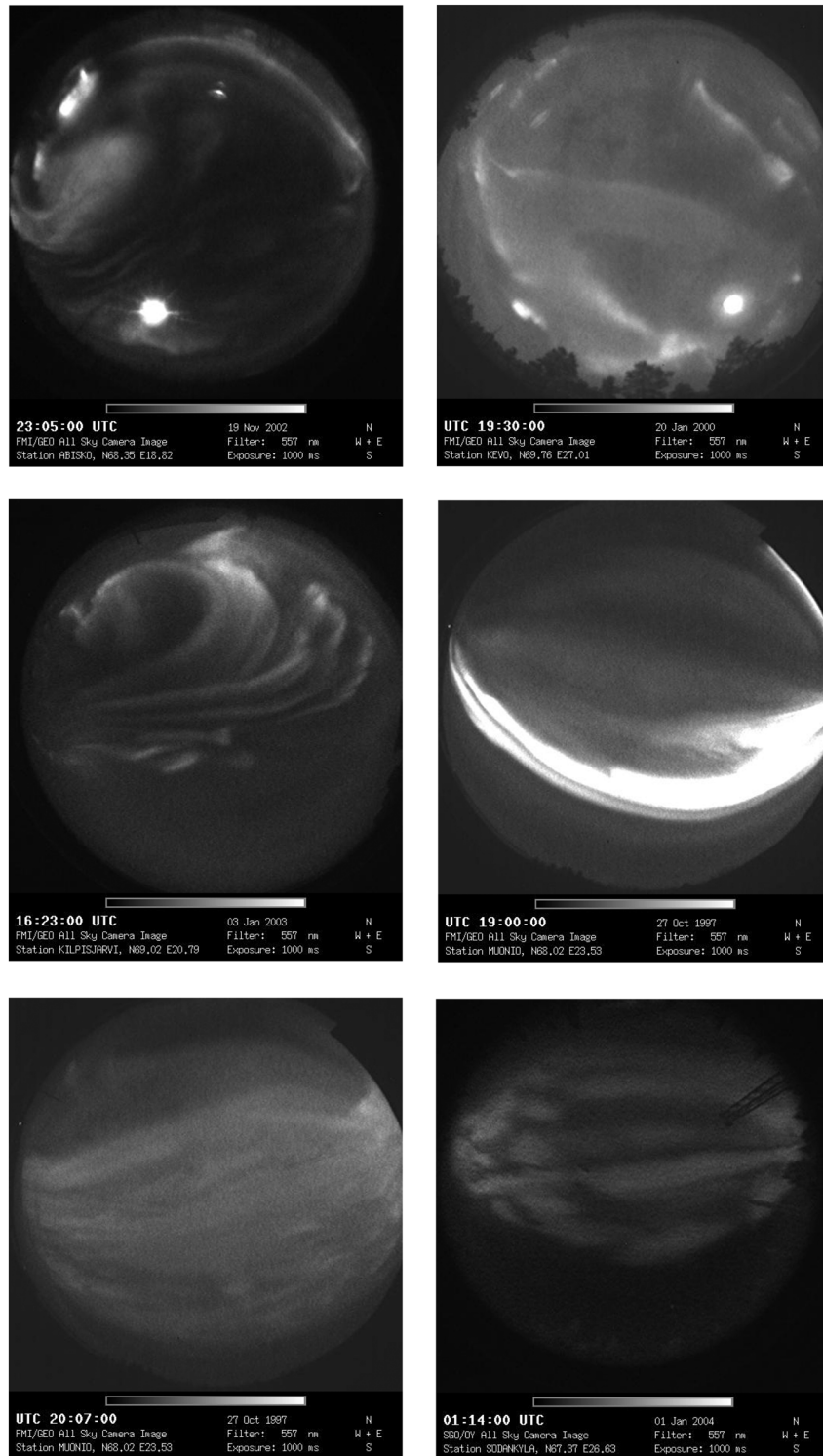


**Figure 9.** Selection of auroral images with arciness values of 0.7–0.8. These displays often include multiple structures with the emission brightness spread over a large part of the field of view.

While well-behaving events can be found, auroral evolution at a neighboring station may look different. Thus, a statistical approach is necessary to determine the bulk behavior. The average substorm onset evolution of the aurora captures the fading of the late growth phase aurora and the change from simpler to more complex structures shortly after the magnetic onset.

The ASC FOVs cover Lapland, while the official  $IL$  index includes all IMAGE stations from Estonia to Svalbard. According to *Tanskanen et al.* [2002], most substorms in the Fennoscandian sector occur in the Lapland latitudes, i.e., over the camera stations used in this study. North of Lapland and over the Arctic Sea the magnetometer network is very sparse up until the Svalbard archipelago, where substorm activity is less frequent. Over 91% of substorms observed in the UV images of the IMAGE spacecraft [*Frey et al.*, 2004] have been reported to be confined between the magnetic latitudes of  $60^\circ$  and  $70^\circ$ , which is consistent with the common FOV of MIRACLE ASCs in Lapland. We analyzed the arciness data set using the official  $IL$  index as a substorm phase identifier, in addition to  $IL_{ASC}$ . The statistical results were not significantly different but including the magnetic substorm signatures outside the FOV of Lapland ASCs introduces a somewhat longer delay between the magnetic onset and auroral breakup.

The median lifetime of arc events is slightly longer during growth phases than during other substorm phases, while the arc event waiting time is longest in the substorm expansion phase. Due to fast fluctuations in arciness and the sparse nature of detected auroral structures, median filtering of the arciness time series is necessary in determining the typical behavior. Missing data in the auroral structure detection relates to decreasing emission brightness, changing weather and daylight conditions (e.g., motion of cloud cover and sunrise/sunset), limited FOV (aurora propagating to or from the ASC FOV), and, to a small extent, also technical problems. In this study, we analyzed individual images of so called paired data set, i.e., auroral structures which were simultaneously detected from two camera stations with overlapping FOVs. Thus, any missing data at one station may cause an image with aurora from a neighboring station become rejected from the analysis. This results in a more limited data set but guarantees its higher quality. There are no moonlit clouds or other artifacts included in the arciness data set when the paired data are required.

The typical lifetimes and waiting times reported here are only slightly dependent on the median filter window size or the length of the missing data allowed in the process. The differences between the substorm phases remain similar. Here we only allow one value less than unity within an arc event and only two values missing (corresponding to a maximum of 1 min between the data points). This results in short-enough lifetimes and waiting times that they are likely to occur within the same substorm phase. Typical arc lifetimes in different substorm phases range from 1.3 min in expansion and recovery to 2 min in the growth phase. With the 20 s cadence of ASC data, this means 4–6 consecutive images of auroral arcs. We do not track individual structures, so there is no guarantee that one arc event consists of a single arc structure, but a small filter window size and a short period of missing data make it more likely that the resulting lifetimes describe the lifetime of individual arc structures as well. Lifetimes of visually identified, discrete, and stable arc structures in ASC images have been estimated to range from 1 min up to several tens of minutes by *Knudsen et al.* [2001] which agrees with the lifetime range of our results. Many case studies of auroral arcs also report lifetimes of the order of a few to several minutes [e.g., *Opgenoorth et al.*, 1990; *Aikio et al.*, 2002]. However, the statistically typical lifetime from our analysis is shorter.

Auroral arcs occupy 8.7% of total growth phase duration, 13.2% of total expansion, and 9.2% of total recovery phase duration. Consequently, the probability of a randomly taken image of an arc being a part of a growth phase is much smaller than it belonging to an expansion phase. This is not surprising when taking into account that the number of observed auroral structures during growth phases is about half of that during expansion and recovery phases. Due to the dynamic nature of expansion phases, auroral structures are bright, and the contrast in the images is good. Although the arciness method is not sensitive to the absolute brightness of the aurora, it does require a good contrast between the aurora (bright pixels) and the background sky. Typically, the required contrast corresponds to aurora detected by a human expert. During the growth phases the average auroral emission intensity is lower [e.g., *Partamies et al.*, 2011] making it harder to reliably identify aurora and detect the structures. In our analysis, the number of detected growth phase structures increased from about 4000 per minute to about 6000 per minute at the end of growth phases, from 10 min prior to the onset to the onset time (data not shown). A similar trend was not observed during the minutes following the onset (at the early expansion phases).

Taking the time difference between the beginning of a growth phase and the first detected arciness value for all growth phases gives a distribution with a mode of 4 minutes. For only 37% of the growth phases the first arciness value was detected within the first 4 min of the phase, while for 75% of the growth phases, the last  $A$  value was detected during the last 4 min of the phase. The arciness data set is sparse everywhere but clearly denser toward the end of the growth phases. This suggests that in most cases the growth phase, as determined from the IMF turning, starts a few minutes earlier than optical aurora can be seen, which partly explains the low number of detected growth phase structures.

The fact that auroral arcs are very common in any substorm phase and in any magnetic activity conditions makes it questionable how meaningful the general division of auroral structures into quiet and active forms is. This may be especially misleading if only single auroral images are considered rather than a time series of auroral evolution. A better parameter would be an occurrence rate of different forms, which includes some information of temporal evolution in the aurora. Quiet, homogeneous, or steady arcs have been frequently observed during substorm growth phases, which is in agreement with our results. However, our findings show that the inverse conclusion in the other way round, that arcs would imply a substorm growth phase or quiet time, is not valid.

As a continuous numeric value for the structural complexity in aurora, arciness may help in understanding the coupling between auroral ionosphere and magnetospheric dynamics. This is especially true for studying the generation mechanisms of different auroral forms. After all, generally known auroral forms only include about 10% of all images containing aurora [Syrjäsuo and Donovan, 2004].

## 6. Conclusions

The occurrence rate of auroral arcs and other structures (arciness, i.e., how arc-like auroral structures appear in all-sky images) during different substorm phases has been observed in northern Fennoscandia in 1996–2007. Our data set of auroral structures captured during substorms includes about 908,000 individual ground-based auroral camera images. The data set of substorms, defined from the local auroral electrojet index calculated from the ASC station magnetometer data ( $I_{L-ASC}$ ), consists of 2650 growth phases, 7188 expansion, and 6635 recovery phases with total durations of 196, 167, and 236 days, respectively.

The shape of the arciness distribution depends very little on the global or local magnetic activity: about one third (20–40%) of the auroral structures are arcs ( $A = 1$ ) in almost any conditions. Only during extreme magnetic activity ( $K_p$  values 8 and 9) is the portion of arcs less than 20% of the auroral structures.

Growth phase arc events typically have a slightly longer lifetime than arc events in the other substorm phases. Still, even the growth phase arc event lifetime is typically only about a couple of minutes. The arc expectation time, on the other hand, is longest during expansion phases due to the highly dynamic auroral displays. A majority of arc events (over 2/3) end when arcs change to more complex structures in any substorm phase, not only during substorm expansion displays.

The time difference between the beginning of the magnetic growth and the first detected arciness value suggests that the magnetic growth typically starts a few minutes earlier than any well-defined optical aurora appears. More importantly, arcs have been observed during 8.7% of the growth phase time, 13.2% of the expansion phase time, and 9.2% of the recovery phase time during auroral imaging seasons. This implies that a randomly selected auroral image of an arc has statistically most likely occurred during a substorm expansion phase, if all the substorm phases were equally likely to happen. This raises a question for future studies of whether arcs in different substorm phases are generated by the same physical processes. Certainly, arcs alone should not be considered signatures of substorm growth phases, and transition of arcs to other forms alone does not imply a substorm onset taking place.

## References

- Aikio, A. T., T. Lakkala, A. Kozlovsky, and P. J. S. Williams (2002), Electric fields and currents of stable drifting auroral arcs in the evening sector, *J. Geophys. Res.*, *107*(A12), 1424, doi:10.1029/2001JA009172.
- Akasofu, S.-I. (1966), The auroral oval, the auroral substorm, and their relations with the internal structure of the magnetosphere, *Planet. Space Sci.*, *14*, 587–595.
- Borovsky, J. (1993), Auroral arc thicknesses as predicted by various theories, *J. Geophys. Res.*, *98*, 6101–6138.
- Frey, H. U., S. B. Mende, V. Angelopoulos, and E. F. Donovan (2004), Substorm onset observations by IMAGE-FUV, *J. Geophys. Res.*, *109*, A10304, doi:10.1029/2004JA010607.

### Acknowledgments

The authors thank S. Mäkinen, J. Mattanen, A. Ketola, T. Raita, and C.-F. Enell for careful maintenance of the camera network and data flow. MIRACLE ASC quicklook data are available at [http://www.space.fmi.fi/MIRACLE/ASC/asc\\_keograms\\_00.shtml](http://www.space.fmi.fi/MIRACLE/ASC/asc_keograms_00.shtml) and at GAIA virtual observatory at <http://gaia-vxo.org>, while full resolution image data can be requested from FMI (kirsti.kauristie@fmi.fi). The work of D. Whiter was financially supported by Academy of Finland (grant 128553). Solar wind and interplanetary magnetic field data were downloaded from OMNI Web at <http://omniweb.gsfc.nasa.gov/> and  $K_p$  index data from the World Data Center for Geomagnetism in Kyoto at <http://wdc.kugi.kyoto-u.ac.jp>.

Larry Kepko thanks Roger Smith and one anonymous reviewer for their assistance in evaluating this paper.

- Gillies, D. M., D. J. Knudsen, E. F. Donovan, E. L. Spanswick, C. Hansen, D. Keating, and S. Erion (2014), A survey of quiet auroral arc orientation and the effects of the interplanetary magnetic field, *J. Geophys. Res. Space Physics*, *119*, 2550–2562, doi:10.1002/2013JA019469.
- Juusola, L., K. Kauristie, O. Amm, and P. Ritter (2009), Statistical dependence of auroral ionospheric currents on solar wind and geomagnetic parameters from 5 years of CHAMP satellite data, *Ann. Geophys.*, *27*, 1005–1017. [Available at [www.ann-geophys.net/27/1005/2009/](http://www.ann-geophys.net/27/1005/2009/).]
- Juusola, L., N. Østgaard, E. Tanskanen, N. Partamies, and K. Snekvik (2011), Earthward plasma sheet flows during substorm phases, *J. Geophys. Res.*, *116*, A10228, doi:10.1029/2011JA016852.
- Kauristie, K., T. I. Pulkkinen, R. J. Pellinen, P. Janhunen, A. Huuskonen, A. Viljanen, H. J. Opgenoorth, W. J. Heikkilä, and D. N. Baker (1995), Analysis of the substorm trigger phase using multiple ground-based instrumentation, *Geophys. Res. Lett.*, *22*, 2065–2068.
- Kauristie, K., T. I. Pulkkinen, R. J. Pellinen, and H. J. Opgenoorth (1996), What can we tell about global auroral-electrojet activity from a single meridional magnetometer chain?, *Ann. Geophys.*, *14*, 1177–1185, doi:10.1007/s00585-996-1177-1.
- Kauristie, K., M. Syrjäsoo, O. Amm, A. Viljanen, T. Pulkkinen, and H. Opgenoorth (2001), Statistical study of evening sector arcs and electrojets, *Adv. Space Res.*, *28*, 1611–1616.
- Knudsen, D., E. Donovan, L. Cogger, B. Jackel, and W. Shaw (2001), Width and structure of mesoscale optical auroral arcs, *Geophys. Res. Lett.*, *28*, 705–708.
- Opgenoorth, H. J., I. Haggstrom, P. J. S. Williams, and G. O. L. Jones (1990), Regions of strongly enhanced perpendicular electric fields adjacent to auroral arcs, *J. Atmos. Terr. Phys.*, *52*, 449–458, doi:10.1016/0021-9169(90)90044-N.
- Partamies, N., K. Kauristie, T. I. Pulkkinen, and M. Brittnacher (2001), Statistical study of auroral spirals, *J. Geophys. Res.*, *106*(A8), 15,415–15,428, doi:10.1029/2000JA900172.
- Partamies, N., M. Syrjäsoo, and E. Donovan (2007), Using colour in auroral imaging, *Can. J. Phys.*, *85*, 101–109, doi:10.1139/P06-090.
- Partamies, N., L. Juusola, E. Tanskanen, K. Kauristie, J. M. Weygand, and Y. Ogawa (2011), Substorms during different storm phases, *Ann. Geophys.*, *29*, 2031–2043, doi:10.5194/angeo-29-2031-2011.
- Partamies, N., L. Juusola, E. Tanskanen, and K. Kauristie (2013), Statistical properties of substorms during different storm phases, *Ann. Geophys.*, *31*, 349–358, doi:10.5194/angeo-31-349-2013.
- Partamies, N., D. Whiter, M. Syrjäsoo, and K. Kauristie (2014), Solar cycle and diurnal dependence of auroral structures, *J. Geophys. Res. Space Physics*, *119*, 8448–8461, doi:10.1002/2013JA019631.
- Sangalli, L., N. Partamies, M. Syrjäsoo, C.-F. Enell, K. Kauristie, and S. Mäkinen (2011), Performance study of the new EMCCD-based all-sky cameras for auroral imaging, *Int. J. Remote Sens.*, *32*, 2987–3003, doi:10.1080/01431161.2010.541505.
- Stringer, W., and A. Belon (1967), The morphology of the ISQY Auroral Oval 2. Auroral alignments in and near the auroral oval, *J. Geophys. Res.*, *72*, 4423–4429.
- Syrjäsoo, M., and E. F. Donovan (2004), Diurnal auroral occurrence statistics obtained via machine vision, *Ann. Geophys.*, *22*, 1103–1113, doi:10.5194/angeo-22-1103-2004.
- Syrjäsoo, M., et al. (1998), Observations of Substorm Electrodynamics Using the MIRACLE Network, in *Proceedings of the International Conference on Substorms-4, Lake Hamana, Japan, 9–13 March*, edited by S. Kokubun and Y. Kamide, pp. 111–114, Terra Sci., Tokyo.
- Tanskanen, E., T. I. Pulkkinen, H. E. J. Koskinen, and J. A. Slavin (2002), Substorm energy budget during low and high solar activity: 1997 and 1999 compared, *J. Geophys. Res.*, *107*(A6), 1086, doi:10.1029/2001JA900153.
- Wang, Q., J. Liang, Z.-J. Hu, H.-H. Hu, H. Zhao, H.-Q. Hu, X. Gao, and H. Yang (2010), Spatial texture based automatic classification of dayside aurora in all-sky images, *J. Atmos. Sol. Terr. Phys.*, *72*, 498–508, doi:10.1016/j.jastp.2010.01.011.
- Whiter, D. K., B. Gustavsson, N. Partamies, and L. Sangalli (2013), A new automatic method for estimating the peak auroral emission height from all-sky camera image, *Geosci. Instrum. Method. Data Syst.*, *2*, 131–144, doi:10.5194/gi-2-131-2013.